Available online at www.sciencedirect.com
ScienceDirect
Procedia Engineering 2 (2010) 2431–2436
Procedia Engineering
www.elsevier.com/locate/procedia

8th Conference of the International Sports Engineering Association (ISEA)

Aerodynamic Characteristics and Flow Pattern of a Golf Ball with Rotation

Katsumi Aoki[a,*], Koji Muto[b], Hiroo Okanaga[a]

[a]*Tokai university, Department of mechanical engineering, School of engineering, 1117 Kitakaname Hiratsuka Kanagawa, 259-1292, Japan*
[b]*Tokai university,Graduate student, Course of mechanical engineering,Graduate school of engineering, 1117 Kitakaname Hiratsuka Kanagawa, 259-1292, Japan*

Received 31 January 2010; revised 7 March 2010; accepted 21 March 2010

Abstract

The present study investigated the aerodynamic characteristics and flow pattern of a golf ball with 328 circular arc dimples. The aerodynamic forces and the flow pattern around a golf ball were investigated experimentally. The detailed flow pattern around a golf ball was then investigated computationally by Large eddy simulation. The aerodynamic characteristics and the flow pattern of a golf ball with rotation were clarified. In addition, the flying distance was clarified through a flying simulation based on the aerodynamic forces and the flow pattern.

Keywords: Golf ball; Dimple; Rotation; Aerodynamic characteristics; Flow pattern; Flow visualization; CFD

1. Introduction

It is known that the flying distance of a golf ball is affected by the initial condition (initial velocity, launcher angle and rotation rate) at the time of impact and the aerodynamic characteristics (drag and lift) during the flying time. Bearman and Harvey (1976) and Smits and Smith (1994) investigated the drag and lift characteristics and the spin rate decay of a golf ball. Ting (2004) investigated the effects of dimple width and dimple depth on the aerodynamic characteristics for a golf ball by CFD. Aoki *et al.* (2003 and 2004) investigated the effects of dimple number, dimple depth and dimple shape on the aerodynamic characteristics of a golf ball by experiments and CFD. However, it is difficult to clarify the flow pattern around a golf ball because the flow pattern associated with the dimpled surface is extremely complicated. The purpose of the present study is to clarify the relationship between the aerodynamic characteristics and the flow pattern of a golf ball with rotation. The aerodynamic forces (drag and lift) and the flow pattern around a golf ball are investigated experimentally. The detailed flow pattern around a golf ball is then clarified computationally by Large eddy simulation. The aerodynamic characteristics and the flow pattern of

*Corresponding author. Tel.: +81-463-58-1211 ; fax: +81-463-59-2207.
E-mail address: katumi@keyaki.cc.u-tokai.ac.jp.

1877-7058
doi:10.1016/j.proeng.2010.04.011

a golf ball with rotation are clarified by the experimentally and computationally results. In addition, the flying distance is clarified through a flying simulation based on the aerodynamic forces and the flow pattern.

2. Experimental apparatus and methods

2.1. Test golf ball

The test golf ball is made of vinyl chloride. The diameters of the test golf balls (d) are 42.6 and 100mm. Figure 1 shows the dimples in section. In the present study, the dimples are in the form of circular arc. The depth ratio of dimple (k/d) (k : depth of dimple) is 0.0079, and the width ratio of dimple (c/d) (c : width of dimple) is 0.0828. A total of 328 dimples are distributed uniformly over the test golf ball.

2.2. Measurement of aerodynamic forces and flow visualization

The blow-down type wind tunnel having a test section of 400×400mm is used for aerodynamic measurements and flow visualization of the test golf ball. The free stream velocity (U) is varied from 10 to 60m/s. The turbulence intensity in this velocity range is 0.3%. The Reynolds number ($Re=Ud/v$, v : kinematic viscosity) based on the free stream velocity and the diameter of the test golf ball is from 0.4×10^5 to 1.7×10^5. Figure 2 shows the outline of the equipment used to measure the drag force (D) and lift force (L). The dimensions of the frame are 500×500mm, and the frame is placed 100mm from the outlet of the wind tunnel. The test golf ball is fixed at the center of the frame using piano wire to provide tension at both fixed ends. The rotation rate (N) is changed by adjusting the voltage of a motor connected to the piano wire. The drag and lift on the test golf ball are measured by a three component load cell with a strain gage attached below the frame. Based on these drag and lift values, the drag coefficient (C_D) and lift coefficient (C_L) are calculated using Eq. (1) and Eq. (2) respectively. Here, the spin rate (α) is the dimension less value obtained by dividing the circumferential velocity (V) by the free stream velocity. In addition, the pressure coefficient (C_P) (used in Figure 5) is the dimension less value obtained by dividing the static pressure by the dynamic pressure. The flow pattern around the test golf ball is then visualized by the spark tracing method.

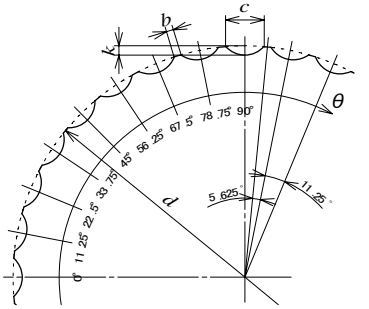

Fig.1. Equatorial section of test golf ball

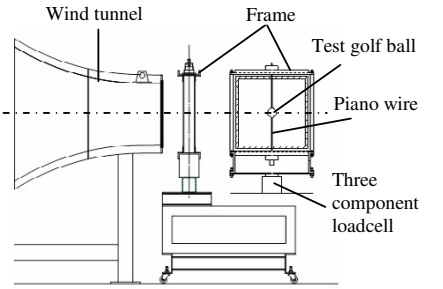

Fig.2. Outline of experimental apparatus

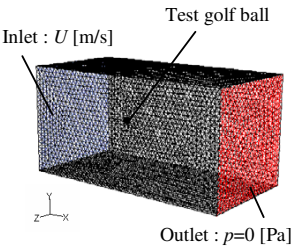

Fig.3. Analysis domain

$$C_D = \frac{D}{A \cdot (\rho \cdot U^2 / 2)} \quad (1) \qquad C_L = \frac{L}{A \cdot (\rho \cdot U^2 / 2)} \quad (2) \qquad \alpha = \frac{V}{U} \quad (3) \qquad C_P = \frac{P - P_0}{\rho \cdot U^2 / 2} \quad (4)$$

D : Drag force on a golf ball [N] L : Lift force on a golf ball [N] P : Pressure on a golf ball surface [Pa]

U : Free stream velocity [m/s] ρ : Density of air [kg/m^3] P_o : Pressure of free stream velocity [Pa]

A : Projected area [m^2] V : Circumferential velocity [m/s]

3. Computer Fluid Dynamics (CFD)

General-purpose thermal fluid analysis software (FLUENT) for Large eddy simulation is used for the computation. Figure 3 shows the analysis domain. Non-structural triangular meshes are mapped on the test golf ball

surface. Non-structural prism meshes are used near the test golf ball surface, and Non-structural tetrahedral meshes are used in other spaces. There are approximately one and a half million meshes in the analysis domain. The dimensions of analysis domain are $40d^{L}\times 20d^{W}\times 20d^{H}$, and the test golf ball is placed $10d$ from the inlet section. The Reynolds number (Re) based on the free stream velocity and the diameter of the test golf ball is Re=1.27×10^5.

4. Results and Considerations

4.1. Aerodynamic forces on a golf ball

Figure 4 shows the drag coefficient (C_D) with the variation of Reynolds number (Re). The C_D of the smooth ball is constant at approximately C_D=0.45 for any Re and in the sub critical region. On the other hand, the C_D of the golf ball varies significantly with Re. The change from the sub critical region to the critical region occurs at approximately Re=0.5×10^5. At this Re, the C_D decreases suddenly to approximately C_D=0.25. The dimples on the surface of the ball cause the critical region of the golf ball to shift a lower Re compared to that of the smooth ball. Figure 5 shows the drag coefficient (C_D) and lift coefficient (C_L) with the variation of the spin rate (α) for the case in which Re=1.27×10^5. This Re corresponds to the free stream velocity of U=45m/s and the α range (from 0 to 0.2) corresponds to the rotation rate range (from 0 to 4000rpm). The C_D of the smooth ball is large, and the C_L of the smooth ball becomes negative in this α range. This phenomenon has reported to occur as a result of the negative magnus force acting on the smooth ball in this α range (Taneda, 1957). On the other hand, the C_D of the golf ball is smaller than that of the smooth ball in this α range. Then, as α increases, both the C_D and C_L of the golf ball increase.

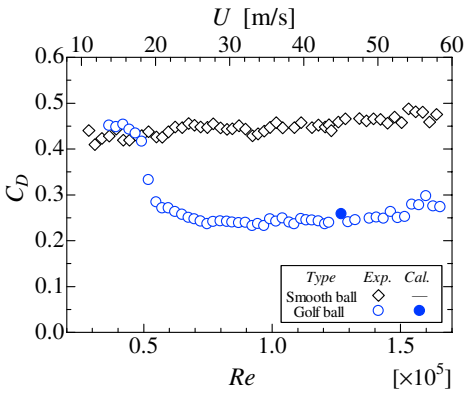

Fig.4. Drag coefficients (without rotation)

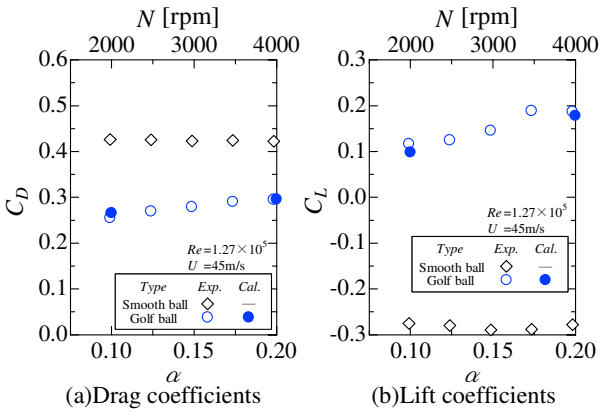

(a)Drag coefficients (b)Lift coefficients

Fig.5. Drag and lift coefficients (with rotation)

4.2. Flow visualizations around a golf ball

Figure 6 (1) shows the flow visualizations around the smooth ball and the golf ball without rotation obtained by the spark tracing method for the case in which Re=1.27×10^5. The flow is from left to right. For the case of smooth ball, the separation point is in the vicinity of θ=80°, and the wake region is large. On the other hand, the separation point of the golf ball is shifted downstream compared to that of the smooth ball, and the wake region of the golf ball is smaller than that of the smooth ball. As shown in Figure 4, the C_D of the golf ball is smaller than that of the smooth ball. The separated flow then flows backward in the wake region. In addition, Figure 6 shows the contours of the pressure coefficient distribution on the golf ball obtained by the computation. The separation point in the pressure coefficient distribution exhibits the same tendency as the flow visualization result. The pressure of outside the dimple is smaller than that of inside the dimple, which indicates that the velocity of outside the dimple is higher than that of inside the dimple.

Figures 6 (2) and (3) show the flow visualizations around the smooth ball and the golf ball with rotation (clockwise direction) obtained by the spark tracing method for the case in which Re=1.27×10^5. The acceleration side of the flow is from 0° to 180° and the deceleration side of flow is from 180° to 360°. The separation points are

located symmetrically on the acceleration and deceleration sides for the case without rotation. However, the separation points are located asymmetrically on the acceleration and deceleration sides for the case with rotation. In case of the smooth ball, the separation point on the deceleration side shifts downstream compared to that on the acceleration side. The wake region of the smooth ball then shifts counterclockwise. As shown in Figure 5, the C_L of the smooth ball becomes negative in this α range. On the other hand, in case of the golf ball, the separation point on the acceleration side shifts downstream compared to that on the deceleration side. The wake region of the golf ball then shifts clockwise (in the direction of rotation) and is smaller than that of the smooth ball. As α increases, the separation point on the acceleration side shifts downstream and the separation point on the deceleration side shifts upstream. As shown in Figure 5, the C_D and C_L become larger as α increases. In addition, the separation point in the pressure distribution exhibits the same tendency as the flow visualization results. The pressure on the acceleration side is smaller than that on the deceleration side. Therefore, as a result of the pressure differential between the acceleration side and deceleration side, a lift force acts on the golf ball from the deceleration side to the acceleration side.

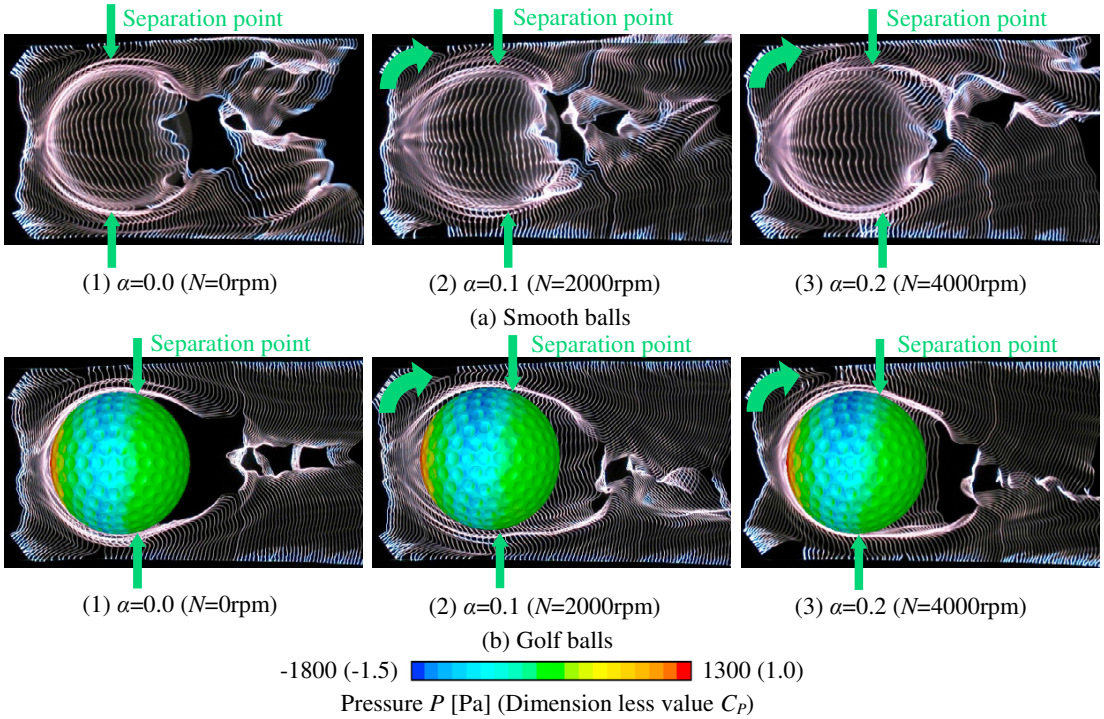

Fig.6. Flow visualizations around the smooth ball and the golf ball by the spark tracing method

Figure 7 shows the flow visualizations around the golf ball with and without rotation (clockwise direction) obtained by the computation for the case in which Re=1.27×10^5. The flow is from left to right. Figure 7 (a) shows the velocity vectors (lateral view) around the golf ball. For the case without rotation, the magnitude of the velocity around the golf ball exhibits the same tendency on the acceleration and deceleration sides. Therefore, the separation points are located symmetrically on the acceleration and deceleration sides. However, as α increases, the magnitude of the velocity around the golf ball on the acceleration side is larger than that on the deceleration side, and the separation point on the acceleration side is shifted downstream compared to that on the deceleration side. Therefore, the wake region shifts clockwise (in the direction of rotation) as α increases. The separated flow then flows backward at low velocity and forms vortices in the wake region. Figure 7 (b) shows the velocity vectors (rear view) around the golf ball. For the case without rotation, the wake region does not shift clockwise (in the direction of rotation) because the separation points are located symmetrically on the acceleration and deceleration sides. However, as α increases, the flow on the acceleration side shifts downstream, and the wake region shifts clockwise (in the direction of rotation). Figure 7 (c) shows the path lines around the golf ball. The wake region shifts clockwise

(in the direction of rotation) as α increases, and the separated flow forms vortices in the wake region. Therefore, as a result of the velocity differential (caused by the pressure differential shown in Figure 6) between the acceleration side and deceleration side, a lift force acts on the golf ball from the deceleration side to the acceleration side.

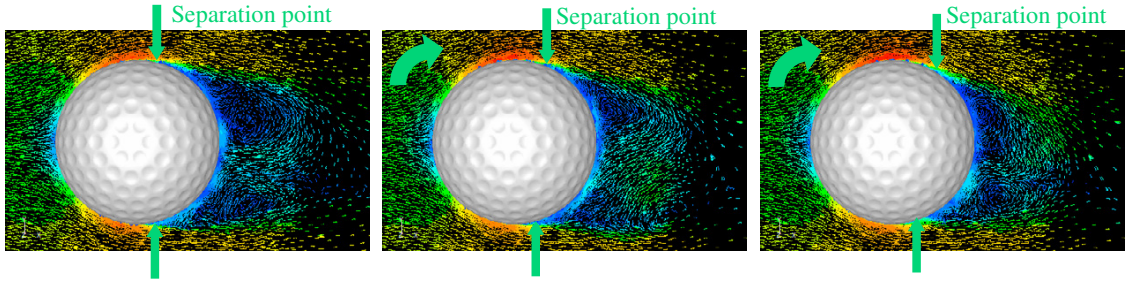

(1) α=0.0 (N=0rpm) (2) α=0.1 (N=2000rpm) (3) α=0.2 (N=4000rpm)

(a) Velocity vectors (Lateral view)

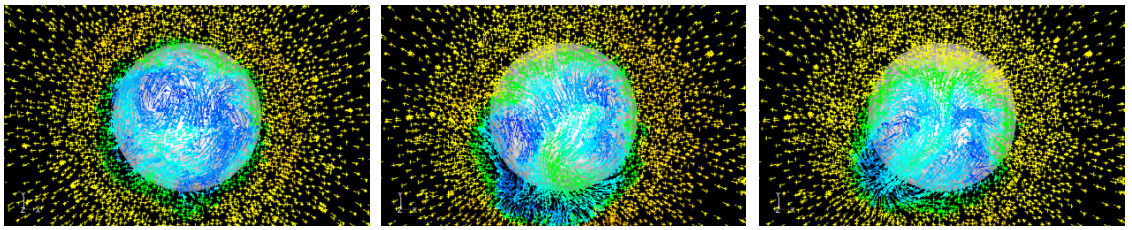

(1) α=0.0 (N=0rpm) (2) α=0.1 (N=2000rpm) (3) α=0.2 (N=4000rpm)

(b) Velocity vectors (Rear view)

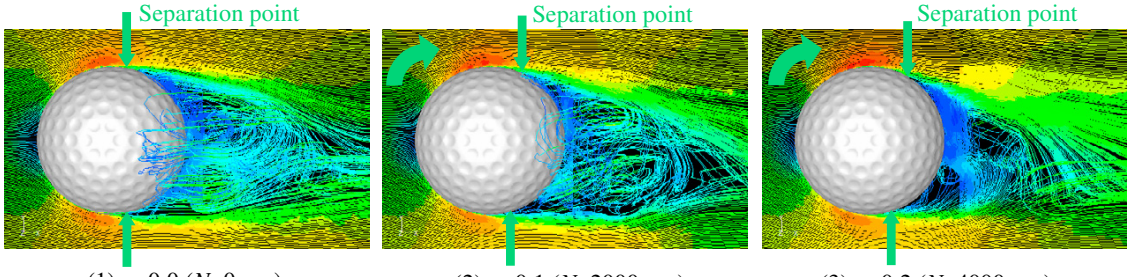

(1) α=0.0 (N=0rpm) (2) α=0.1 (N=2000rpm) (3) α=0.2 (N=4000rpm)

(c) Path lines

Velocity magnitude u [m/s] (Dimension less value u/U)

Fig.7. Flow visualizations around the golf ball by the computation

5. Flying simulations

Figure 8 shows the flying simulation. The flying distance is simulated using the C_D and C_L obtained from the above results. Figure 8 (a) shows the results of simulating the change in the flying distance without rotation for the case in which Re=1.27×10^5 (U=45m/s). The flying distance without rotation depends on the C_D. The golf ball flies farther than the smooth ball because the drag force on the golf ball is smaller than that of the smooth ball, as shown in Figure 4. Figure 8 (b) shows the results of simulating the change in the flying distance with rotation (α=0.2) for the case in which Re=1.27×10^5 (U=45m/s). The flying distance with rotation depends on the C_D and C_L. The large drag force acts on the smooth ball, and the lift force on the smooth ball acts downward, as shown in Figure 5. Therefore, the flying distance of the smooth ball is short. On the other hand, the drag force on the golf ball is smaller than that on the smooth ball, and the lift force on the golf ball acts upward, as shown in Figure 5. Therefore, the flying distance of the golf ball is farther than that of the smooth ball. Figure 9 shows the flying distance of the golf

ball with the variation of α. As α increases, the lift force increases, as shown in Figure 5. Therefore, the flying distance and the altitude of the golf ball increase as α increases.

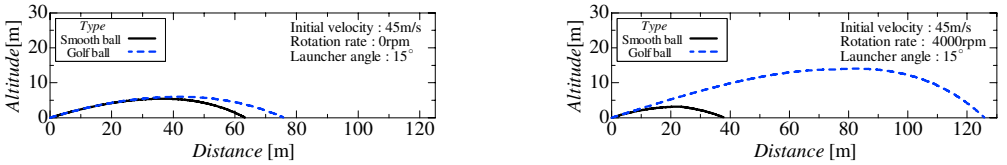

(a) Without rotation (α=0.0 (N=0rpm)) (b) With rotation (α=0.2 (N=4000rpm))

Fig.8. Flying simulations of the smooth ball and the golf ball with and without rotation

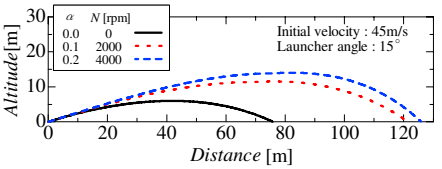

Fig.9. Flying simulations of the golf ball with the variation of spin rate

6. Conclusions

By investigating the aerodynamic characteristics and the flow pattern of a golf ball both experimentally and computationally, the following conclusions were obtained.

(1) The critical region of a golf ball shifts toward a lower *Re* compared to that of a smooth ball. Therefore, the drag coefficient of a golf ball is smaller than that of a smooth ball.

(2) As the spin rate increases, the lift coefficient of a smooth ball becomes negative, whereas the drag and lift coefficients of a golf ball increase.c

(3) For the case without rotation, the separation point of a golf ball shifts downstream compared to that of a smooth ball. Therefore, the drag coefficient of a golf ball becomes smaller than that of a smooth ball.

(4) For the case of a smooth ball, the separation point on the deceleration side shifts downstream compared to that on the acceleration side. Therefore, the lift coefficient becomes negative. On the other hand, for the case of a golf ball, the separation point on the acceleration side shifts downstream compared to that on the deceleration side. Therefore, the lift coefficient becomes positive.

(5) A flying simulation revealed that a flying distance depends on the aerodynamic forces. For the case without rotation, a golf ball flies farther than a smooth ball because the drag force on a golf ball is smaller than that on a smooth ball. For the case with rotation, a flying distance of a smooth ball is short because the drag force acting on a smooth ball is large and the lift force on a smooth ball acts downward. On the other hand, a flying distance of a golf ball is farther because the drag force on a golf ball is smaller than that on a smooth ball and the lift force acts upward.

References

[1] Bearman P.W. and Harvey J.K. (1976) Golf ball aerodynamics. *Aeronautical Quarterly*, 27, 112-122.

[2] Smits A.J. and Smith D.R. (1994) A new aerodynamics model of a golf ball in flight. *Science and Golf*, Ⅱ, 340-347.

[3] Ting L.L. (2004) Effects of dimple size and depth on golf ball aerodynamic performance. *4th ASME-JSME Joint Fluids Engineering Conference*, 1-7.

[4] Aoki K., Ohike A., Yamaguchi K. and Nakayama Y. (2003) Flying characteristics and flow pattern of a sphere with dimples. *Journal of visualization*, Vol.6, No.1, 67-76.

[5] Aoki K., Nonaka M. and Goto T. (2004) Aerodynamic and flying characteristics for the surface structure on the golf ball. *Proceedings of the school of Engineering Tokai University*, Vol.44, No.2, 67-72.

[6] Taneda S. (1957) Negative magnus effect. *Reports of Research Institute for Applied Mechanics*, Vol.V, No.20, 123-128.